Analysis of Grain Structure in Partially Ordered Block Copolymers by Depolarized Light Scattering and Transmission Electron Microscopy

M. Y. Chang,[†] F. M. Abuzaina,[†] W. G. Kim,[†] J. P. Gupton,[†] B. A. Garetz,*[,†] M. C. Newstein,[†] N. P. Balsara,*[,‡] L. Yang,[§] S. P. Gido,[§] R. E. Cohen,[⊥] Y. Boontongkong,[#] and A. Bellare[&]

Department of Chemical Engineering and Chemistry and Department of Electrical Engineering, Polytechnic University, Brooklyn, New York 11201; Department of Chemical Engineering, University of California, Berkeley, California 94720; Department of Polymer Science and Engineering, University of Massachusetts, Amherst, Massachusetts 01003; Department of Chemical Engineering, Massachusetts Institute of Technology, Cambridge, Massachusetts 02139; Department of Materials Science and Engineering, Massachusetts Institute of Technology, Cambridge, Massachusetts 02139; and Department of Orthopedic Surgery, Harvard Medical School, Boston, Massachusetts 02115

Received January 22, 2002

ABSTRACT: The grain structure in lamellar block copolymer samples undergoing a disorder-to-order transition was studied by a combination of depolarized light scattering (DPLS) and transmission electron microscopy (TEM). The 4-fold symmetry of the DPLS profiles indicated the presence of anisotropic grains. A pattern recognition algorithm for analyzing the TEM micrographs of samples partially filled with anisotropic, ordered grains was developed. The volume fractions of sample occupied by ordered grains determined from light scattering and electron microscopy are in reasonable agreement. Both methods indicate that, on average, the characteristic length of the grains in the direction perpendicular to the lamellar planes was a factor of 2 larger than that in the plane of the lamellae. The absolute magnitudes of grain sizes determined by light scattering are about 50% larger than those determined by microscopy.

1. Introduction

Block copolymer materials self-assemble into a variety of periodic ordered structures when cooled below the order−disorder transition temperature.[1] In this paper we focus on the lamellar phase formed by symmetric diblock copolymers, which has been characterized by a combination of techniques such as transmission electron microscopy and small-angle X-ray scattering.[1−6] The data obtained in position space by microscopy are complementary to the data obtained in reciprocal space by scattering. The factors that control the average lamellar spacing have been studied extensively, and the agreement between position and reciprocal space data is excellent.

Ordered samples formed in the absence of external fields consist of randomly oriented grains with concomitant defects; coherent order is restricted to regions within individual grains. Grains composed of lamellae exhibit form birefringence, with an optic axis normal to the lamellar planes. Grain structure plays an important role in determining the mechanical and transport properties of block copolymer materials.[7−9] Controlling grain structure is essential if block copolymers are to be used in electronic and photonic applications.[10,11] The purpose of this paper is to characterize the grain structure of lamellar block copolymers in both position and reciprocal space.

Analysis of grain structure is considerably more challenging than the analysis of lamellar spacing. The distribution of lamellar spacings is sharply peaked at a value d. This is due to the fact that the lamellar spacing is determined by equilibrium thermodynamics. It is usually adequate to consider the lamellar spacing of a sample to be a constant. In contrast, grain structure is determined by nonequilibrium processes such as nucleation, grain growth, and defect annihilation. This leads to a broad distribution of grain sizes, and there are no predictions for the functional form of this distribution. It is much more difficult to measure a broad distribution of length scales than a single parameter such as d. Additional difficulties arise due to the liquid crystalline character of lamellae; the correlation lengths along and perpendicular to the director need not be identical. Characterization of the grain structure of some lamellar samples thus requires specifying two broad distributions of length scales.

Myers et al. have proposed that the grain structure of lamellar block copolymers can be studied in reciprocal space by ultrasmall-angle X-ray scattering.[12] They found an upturn in X-ray scattering at ultralow angles (below 0.1°), indicating the presence of structures with a length scale of 100−1000 nm. They assumed that this signal was due to the electron density difference between grains and grain boundaries and thus estimated average grain sizes from these measurements.

Another reciprocal space method used to study block copolymer grain structure in this study is depolarized light scattering (DPLS).[13−20] Previous studies have shown that DPLS profiles from ordered block copolymers either can be azimuthally symmetric[14,15] or exhibit 4-fold symmetry.[16−20] By introducing simple models for the grain structure, it was shown that azimuthally symmetric scattering patterns are expected if the sample is composed of randomly shaped grains, while patterns

[†] Polytechnic University.
[‡] University of California, Berkeley.
[§] University of Massachusetts.
[⊥] Department of Chemical Engineering, Massachusetts Institute of Technology.
[#] Department of Materials Science and Engineering, Massachusetts Institute of Technology.
[&] Harvard Medical School.
* To whom correspondence should be addressed. E-mail bgaretz@duke.poly.edu and nbalsara@cchem.berkeley.edu.

10.1021/ma0201025 CCC: $22.00
Published on Web 04/27/2002

with 4-fold symmetry are expected if the grains are anisotropic in shape on average, with respect to the optic axis. DPLS was also used to study the kinetics of grain growth after quenching the sample from the disordered to the ordered state.[16−19] The analysis of these data required developing models wherein the sample was only partially filled with ordered grains.

In a previous study,[15] block copolymer samples filled with randomly shaped grains were studied in position and reciprocal space by transmission electron microscopy (TEM) and DPLS, respectively. Grain sizes from TEM data were obtained using a local two-dimensional Fourier analysis. The average grain size determined by DPLS was within a factor of 2 of that obtained from analysis of TEM micrographs. The Fourier analysis methodology was also used to study the grain structure in graft copolymer samples.[21] In a closely related study, Harrison et al. have conducted position space studies of grain structure in two-dimensional block copolymer films supported on silicon substrates.[22,23] They implemented a filtered Fourier transform method for obtaining grain size from position space data, which is analogous to the method developed in ref 15. They demonstrated that annealing the block copolymer films led to an increase in grain size. By conducting time-resolved position space measurements, Harrison et al. and others have identified some of the molecular-scale processes that lead to defect annihilation and grain growth.[23,24]

Transmission electron micrographs of partially ordered block copolymer samples were presented in ref 5 by Sakamoto and Hashimoto. They obtained images of ordered grains coexisting with disordered regions. The borders of a few ordered grains were drawn by hand, and they noted that the chosen grains were anisotropic. However, no quantitative analysis of the micrographs was attempted.

The main purpose of this paper is to present a quantitative analysis of position space TEM data obtained from *partially ordered* samples containing *anisotropic* grains, thereby extending our previous analysis[15] that considered *fully ordered* samples with *isotropic* grains. We first develop quantitative criteria for distinguishing between disordered and ordered regions in TEM micrographs. We then determine the characteristic grain lengths in the direction of the lamellar normals and perpendicular to them. We conclude with a comparison of grain structure determined from TEM and DPLS data.

2. Experimental Section

A polystyrene−polyisoprene diblock copolymer was synthesized by anionic polymerization under high vacuum. The weight-averaged molecular weights of both polystyrene and polyisoprene blocks were determined to be 6 kg/mol, and we refer to this polymer as SI(6−6). The order−disorder transition temperature of SI(6−6) was determined by the birefringence method and found to be 74 ± 1 °C. The sample forms a lamellar structure at temperatures below 74 °C. Differential scanning calorimetry (DSC) measurements on an ordered sample at 10 °C/min indicated that the glass transition temperature (T_g) of the polystyrene lamellae was 68 °C. Our synthesis and characterization procedures are given in ref 25.

Depolarized light scattering measurements were conducted on SI(6−6) melts, using an apparatus and methods described in ref 19. The 1 mm thick SI(6−6) melts were enclosed within optical flats and placed in a thermostated oven, between a polarizer and an analyzer, as shown schematically in Figure 1. The samples were first heated to 87 °C to erase thermal

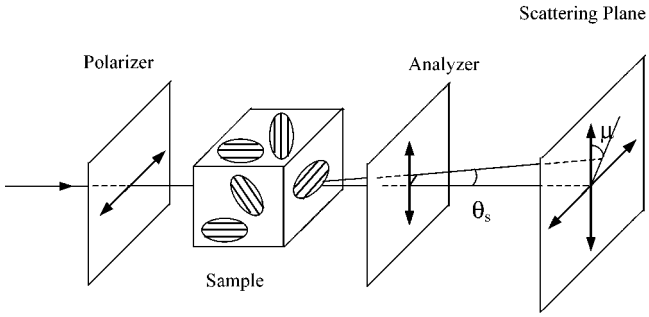

Figure 1. Schematic of the depolarized light scattering experiment with definitions of θ and μ.

history and then rapidly cooled to 72 °C. The samples were tempered at this temperature for different lengths of time, and the depolarized light scattering profiles were monitored during this process. The scattering geometry is defined in Figure 1. The azimuthal angle in the scattering plane, μ, is defined so that $\mu = 0$ corresponds to the direction of the analyzer polarization. The DPLS intensity I along $\mu = 0°$ and 45° was recorded as a function of scattering vector q [$q = 4\pi \sin(\theta_s/2)/\lambda$], where θ_s is the scattering angle and $\lambda = 632$ nm is the wavelength of the incident beam. We present data from two samples, S_{early} and S_{late}, which were tempered for 125 and 350 min, respectively. Time zero is defined as the time at which the temperature change was initiated, and it took about 15 min for the sample temperature to reach 72 °C. After tempering, both samples were cooled rapidly to room temperature. Because the polystyrene lamellae undergo a glass transition at 68 °C, the structure formed at 72 °C is preserved when the samples are cooled to room temperature. Cooling to room temperature had no significant effect on the DPLS profiles. This indicates that our procedure for cooling and trapping the grain structure does not induce artifacts. We note in passing that many SI block copolymer samples with continuous polystyrene phases crack upon cooling to room temperature, presumably due to the stresses that result upon cooling and the fragility of glassy polystyrene. SI block copolymers with continuous polyisoprene phases do not crack upon cooling, but the mobility of the polyisoprene chains may lead to changes in the grain structure during the time between completion of the DPLS experiments and the commencement of the TEM experiments. SI(6−6) was thus ideally suited to the present study. The volume fraction of ordered gains in both S_{early} and S_{late} was kept relatively low (<10%) in order to facilitate the identification of individual grains in position space. In addition, we wanted a clear distinction between the grain structures of S_{early} and S_{late}. We thus obtained the sample S_{early} as soon as the depolarized light scattering signal was significantly larger than the background.

The S_{early} and S_{late} samples were removed from their cells, and ultrathin sections (about 50 nm thickness) were obtained using a Reichert Ultramicrotome at −120 °C. Care was taken to microtome the section of the sample that was in the path of the laser beam in the DPLS experiments. The sections were stained with OsO_4 and examined using a JEOL 1210 transmission electron microscope operated at 100 kV. To get unbiased micrographs, we examined several different sections of the samples and moved the sample stage from one spot to another in a random fashion. Our analysis is based on 53 independent micrographs of the early sample and 56 independent micrographs of the late sample. (Three early-sample micrographs were so underexposed that they contained no detectable contrast; these three images were discarded.) All of the micrographs were obtained using a magnification of 3×10^4.

Before embarking on the microscopy study outlined in the previous paragraph, we conducted several preliminary experiments. We made many versions of S_{early} and S_{late} and obtained micrographs after conducting DPLS experiments. The preliminary TEM experiments were conducted at both the University of Massachusetts and Massachusetts Institute of

Technology. The results obtained in all of the preliminary experiments were in excellent agreement with the results reported in this paper. In our preliminary experiments we noted substantial differences in some of the grain parameters obtained from TEM and DPLS. We decided on the above protocol to ensure, to the best of our ability, that these differences were not due to incomplete sampling.

The parameters used in the "final" experiments that are reported in this paper were based on the results of the preliminary experiments. One of the key decisions concerned magnification. Accurate determination of the local orientation of the lamellae requires high magnification, while obtaining micrographs that encompass entire grains requires low magnification. Our decision to use a magnification of 3×10^4 was a compromise between these two considerations. Our decision to use 53/56 micrographs per sample was based on practical considerations such as limited manpower. Negatives of TEM micrographs, 10 cm × 7 cm in size, were scanned with a resolution of 480 pixels/in. using an Epson 1200C scanner. The digitized data were stored in TIFF files and analyzed using a Fortran program described below. The numerical answers that we have obtained are based on all of the 109 micrographs obtained. The analysis was conducted on the scanned data files without further editing or digital image manipulation. Our approach of using all of the TEM data obtained is quite different from traditional TEM studies wherein "typical" micrographs are displayed without specifying the exact procedure used to select the particular image.

Small-angle X-ray scattering measurements were conducted using beamline 33-ID of the UNICAT facility[25] at the Advanced Photon Source, Argonne National Laboratory. Data were desmeared using the method of Lake.[26,27]

3. Amplitude vs Correlation Methods

We have employed two related procedures for extracting grain parameters from light scattering data, termed the amplitude and correlation methods by Stein.[28] Both assume that the far-field light scattering pattern arises from light diffracted by individual grains. These grains can be characterized by a shape function, $f_i(\mathbf{r})$, which is equal to one when $\mathbf{r}$ lies in the ith grain and zero otherwise. The resulting scattered field amplitude is proportional to the Fourier transform of these shape functions, and the scattered intensity is the square modulus of this amplitude:

$$I(\mathbf{q}) \propto \left|\int d\mathbf{r}' \exp(-i\mathbf{q}\cdot\mathbf{r}') \sum_i f_i(\mathbf{r}')\right|^2 \quad (1)$$

This expression is particularly useful in modeling correlated clusters of grains.[19] Alternatively, this expression can be rewritten as a double integral:

$$I(\mathbf{q}) \propto \int\int d\mathbf{r}'\, d\mathbf{r}'' \exp(-i\mathbf{q}\cdot\mathbf{r}') \exp(i\mathbf{q}\cdot\mathbf{r}'') \sum_i f_i(\mathbf{r}')\, f_i(\mathbf{r}'') \quad (2)$$

Only diagonal terms survive in the sum over i if different grains are assumed to be uncorrelated. This double integral can be reexpressed in terms of the new variables $\mathbf{r}' - \mathbf{r}''$ and $\mathbf{r}' + \mathbf{r}''$, yielding

$$I(\mathbf{q}) \propto \int d(\mathbf{r}' - \mathbf{r}'') \exp[-i\mathbf{q}\cdot(\mathbf{r}' - \mathbf{r}'')] \sum_i f_i(\mathbf{r}')\, f_i(\mathbf{r}'') = \int d\mathbf{r} \exp(-i\mathbf{q}\cdot\mathbf{r})\, C(\mathbf{r}) \quad (3)$$

where the correlation function $C(\mathbf{r}'-\mathbf{r}'') \equiv \sum_i \langle f_i(\mathbf{r}')\, f_i(\mathbf{r}'')\rangle$ is the average over products of shape functions. In this formulation, the scattered intensity is the Fourier transform of a correlation function.

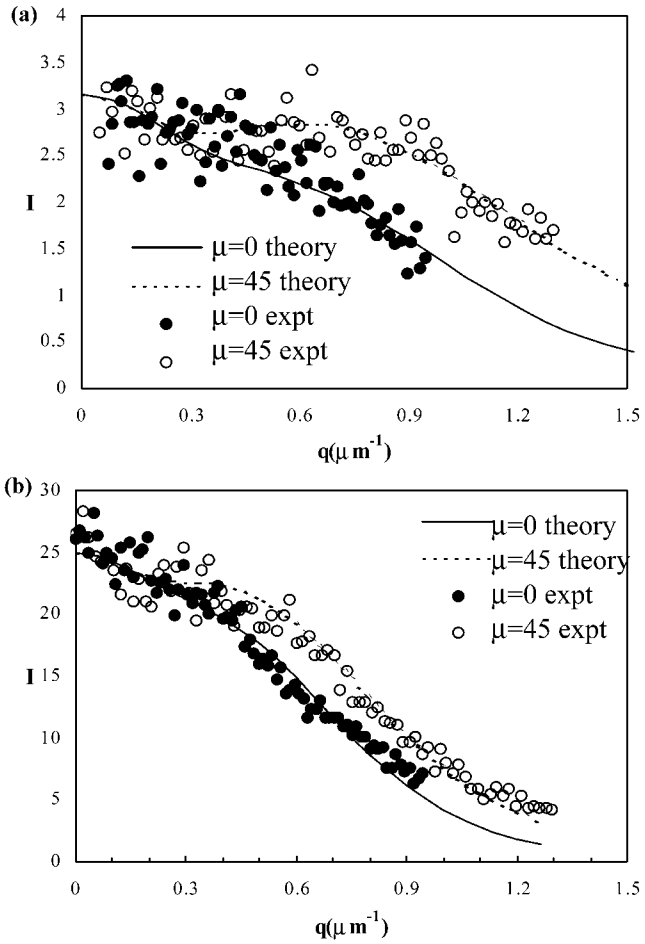

Figure 2. Depolarized light scattering data with theoretical fits from (a) S_{early} and (b) S_{late}. The theoretical curves correspond to (a) $\omega_{\|} = 1.8\ \mu$m, $\omega_{\perp} = 0.9\ \mu$m, and $\Delta = 1.5$ and (b) $\omega_{\|} = 2.4\ \mu$m, $\omega_{\perp} = 1.6\ \mu$m, and $\Delta = 1.5$.

In the modeling of grain parameters, the use of eq 1 is called the amplitude method, whereas use of eq 3 is called the correlation method. For computational convenience, we have usually employed Gaussian functions for both $f(r)$ and $C(r)$. Care must be taken in comparing grain length parameters obtained from these choices. Differences become apparent when we look at the resulting forms of the scattered intensities. For ideal grains, using $f(r) = \exp(-r^2/w_A^2)$ [ref 19] yields $I(q) \propto \exp(-w_A^2 q^2/2)$, while using $C(r) = \exp(-r^2/w_C^2)$ [refs 15 and 16] yields $I(q) \propto \exp(-w_C^2 q^2/4)$. Thus, the different length parameters are related by the equation $w_A = w_C/\sqrt{2}$.

In this paper, we have employed the amplitude method in analyzing our light scattering data, because of the presence of intergrain correlations as evidenced by an off-axis maximum in the scattered light intensity; the details are described in the next section. For the analysis of the TEM micrographs, on the other hand, we have directly computed the lamellar orientation correlation function. In all further discussion in this paper, the Gaussian grain length parameters employed are denoted as $\omega = w_A = w_C/\sqrt{2}$.

4. Analysis of Depolarized Light Scattering Measurements

The DPLS profiles from samples S_{early} and S_{late} are shown in parts a and b of Figure 2, respectively. The scattering profiles obtained from the two samples are

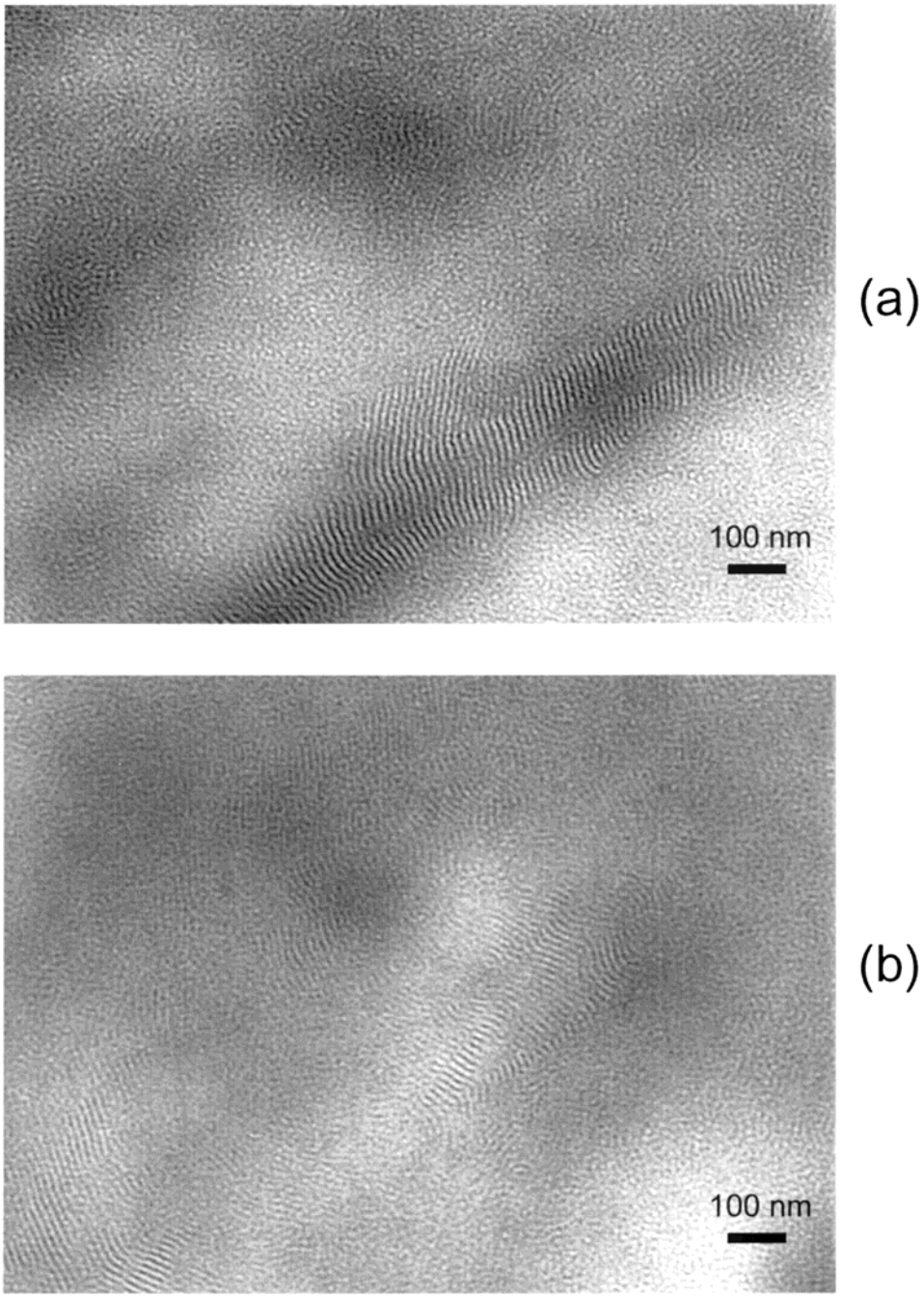

Figure 3. Typical transmission electron micrographs from samples (a) S_{early} and (b) S_{late}.

qualitatively similar. The scattered intensity along $\mu = 45°$ is larger than that along $\mu = 0°$. These data are similar to data published in ref 19. As in ref 19, we use the twisted-H grain model to analyze the data. In this model, the sample is composed of randomly oriented clusters of three anisotropic grains, and the average lengths of the grains in the directions parallel and perpendicular to the optic axis are denoted by $\omega_{||}$ and $\omega_{\perp}$, respectively. Each grain is described by a Gaussian shape function, and details are given in ref 19. It is unreasonable to expect clusters comprising grains of identical size. Experimentally, this would lead to complete extinction of the DPLS signal at $q = 0$, which is not observed (see Figure 2a,b). We thus introduce an additional parameter Δ, which accounts for the polydispersity of grain sizes within a twisted-H cluster. We assume that the middle grain in the twisted-H cluster is a factor $(1 + \Delta)$ longer than the other two grains. The four parameters I_0, $\omega_{||}$, $\omega_{\perp}$, and Δ were varied systematically, and the combination that minimizes the deviation between theory and experiment is reported in the paper (see ref 19 for details). From this analysis, we determine that S_{early} has grains with $\omega_{\perp} = 0.9\ \mu$m and $\omega_{||} = 1.8\ \mu$m, while the S_{late} has grains with $\omega_{\perp} = 1.6\ \mu$m and $\omega_{||} = 2.4\ \mu$m. The parameter Δ used to fit data from both samples was 1.5. The average grain volume, v, in each case is $\omega_{\perp}^2\omega_{||}(1 + \Delta/3)$.

We assume that S_{early} and S_{late} are different due to differences in grain size and grain concentration only. In this case, the scattering intensity as $q \rightarrow 0$, I_0, is proportional to the product of grain volume, v, and the volume fraction of grains, ϕ.[16,19] In refs 16 and 19, the time dependence of ϕ has been investigated in considerable detail. In all systems studied, we have observed that ϕ increases smoothly with time, leveling off at a constant value as $t \rightarrow \infty$. If we use subscripts early and

late to describe parameters corresponding to S_{early} and S_{late}, respectively, then

$$\frac{\phi_{late}}{\phi_{early}} = \frac{I_{0,late}}{I_{0,early}} \frac{v_{early}}{v_{late}} \quad (4)$$

From eq 4 and the data in Figure 2, we obtain $\phi_{late}/\phi_{early} = 1.9$. The rate of order formation (rate of change of ϕ) in SI(6−6) is much slower than that in previous studies[16,19] due to the proximity of the tempering temperature to both the order−disorder transition and T_g.

5. Analysis of Transmission Electron Micrographs

Parts a and b of Figure 3 show typical transmission electron micrographs obtained from S_{early} and S_{late} samples, respectively. OsO_4 selectively stains the polyisoprene lamellae. In both micrographs one observes that they contain ordered lamellar regions indicated by stripes and disordered regions with no stripes. Disordered regions exhibit random fluctuations in composition that have a spatial period comparable to the lamellar spacing in the ordered regions. Note that the volume sampled per micrograph is extremely small: about 1 part in 10^{10} of the illuminated volume in a DPLS experiment. Quantitative information can only be obtained by examination of many micrographs. Further studies are required to ascertain whether our procedure of averaging over 53/56 micrographs per sample is adequate.

Our procedure for extracting the correlation lengths from TEM data builds on the procedure used in ref 15. Each scanned image was divided into 114 by 166 overlapping 56 nm × 56 nm boxes with centers separated by 17.5 nm, and the image within each box was stored as a 32 × 32 element array of 8-bit integers. Our choice of box size represents a compromise between resolution, which requires small boxes, and local structure determination, which is facilitated by boxes whose length is substantially greater than the spatial period of the local structure. Local 2D Fourier transforms (LFTs) were computed for each box, also stored as a 32 × 32 element array of 8-bit integers. A typical micrograph, shown in Figure 4, contains two qualitatively different types of regions: ordered regions that appear as parallel back and white stripes (box 1) and disordered regions that appear as black and white dimples (box 2). Their corresponding LFTs exhibit characteristic patterns that are given in the lower part of Figure 4. All regions exhibit an amplitude peak at zero spatial frequency that is related to the average intensity over the box; this is the central spot in the LFTs in Figure 4. Ordered regions (box 1) exhibit a symmetrical pair of amplitude peaks at finite spatial frequency related to the local period and orientation of the lamellae in the box. Disordered regions (box 2) exhibit a ring of high-amplitude pixels whose radius is related to the principal spatial frequencies associated with the random composition fluctuations in the box. Unclear regions (not pictured) exhibit a symmetrical pair of amplitude peaks that are adjacent to the zero-frequency (dc) peak. Such regions may arise from a number of factors such as holes in the sample, large local thickness of the sample (from uneven microtoming), electron beam damage, obstructing objects on the sample, poor local staining of the sample, or if the region contains lamellae with optic axes perpendicular (or nearly so) to the plane of the micrograph. In S_{early}, 7% of the boxes were unclear, while in S_{late}, 6% of the boxes were unclear.

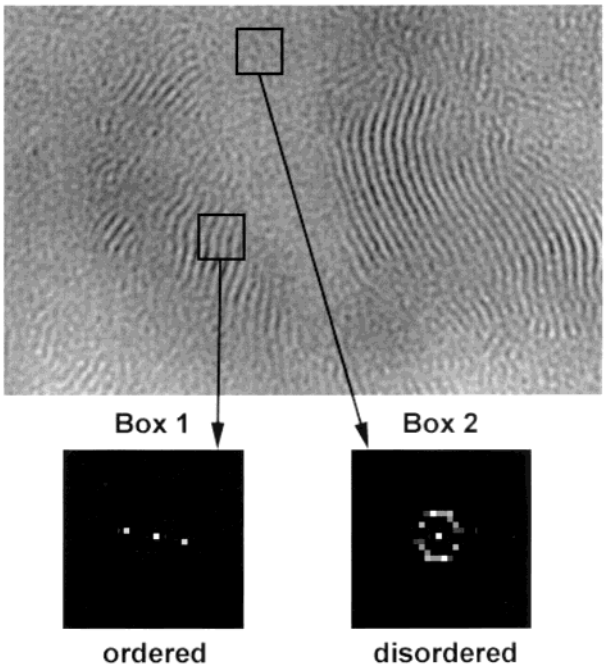

Figure 4. Analysis of transmission electron micrographs using local Fourier transforms (LFTs). (top) Micrograph with ordered and disordered regions. Box 1 contains an ordered region, and box 2 contains a disordered region. (bottom) LFTs of the two boxes, depicting typical local Fourier transforms of ordered and disordered regions.

The following algorithm provides a procedure for distinguishing ordered, disordered, and unclear regions. It is a pattern recognition problem of distinguishing a pair of high-amplitude pixels (ordered box) from a ring of such high-amplitude pixels (disordered box) in Fourier space. In each 32 × 32 LFT array (depicted graphically in the lower part of Figure 4) we locate the symmetric pair of pixels with the largest amplitude (A_{max}) other than the zero-frequency central pixel. We define R_{max} to be the distance (in Fourier space) of these pixels from the zero-frequency pixel, in units of pixels. If this pair of pixels is adjacent to the zero-frequency (center) pixel, we describe the region as unclear. If they are not adjacent to the center pixel, then we have two choices: we label the region either disordered or ordered. To distinguish between these two possibilities, we examined the amplitudes, A, of all other pixels with distance from the center pixel, R, greater than or equal to $R_{max} - 1$ or less than or equal to $R_{max} + 1$. We then calculated the number N of these pixels such that $\log(A)$ is greater than $\log(A_{max}) - 1.5$. We can see in Figure 4 that N/R_{max} is large for the disordered region in box 2 and small for the ordered region in box 1. (Normalization by R_{max} accounts for the increase in ring circumference as R increases.) Thus, if N/R_{max} is greater than a certain prescribed cutoff, then we call the region disordered; otherwise, we call the region ordered. Visual inspection of a variety of boxes suggested that a cutoff value of 2.0 was best for distinguishing ordered and disordered regions. Our results were insensitive to the exact value of the N/R_{max} cutoff in the 1.8−2.2 range.

We now examine quantitative aspects of the two LFT boxes shown in Figure 4. For the LFT of box 1, $\log(A_{max}) = 17.4$, $R_{max} = 5.1$, and $N = 2$. The value of

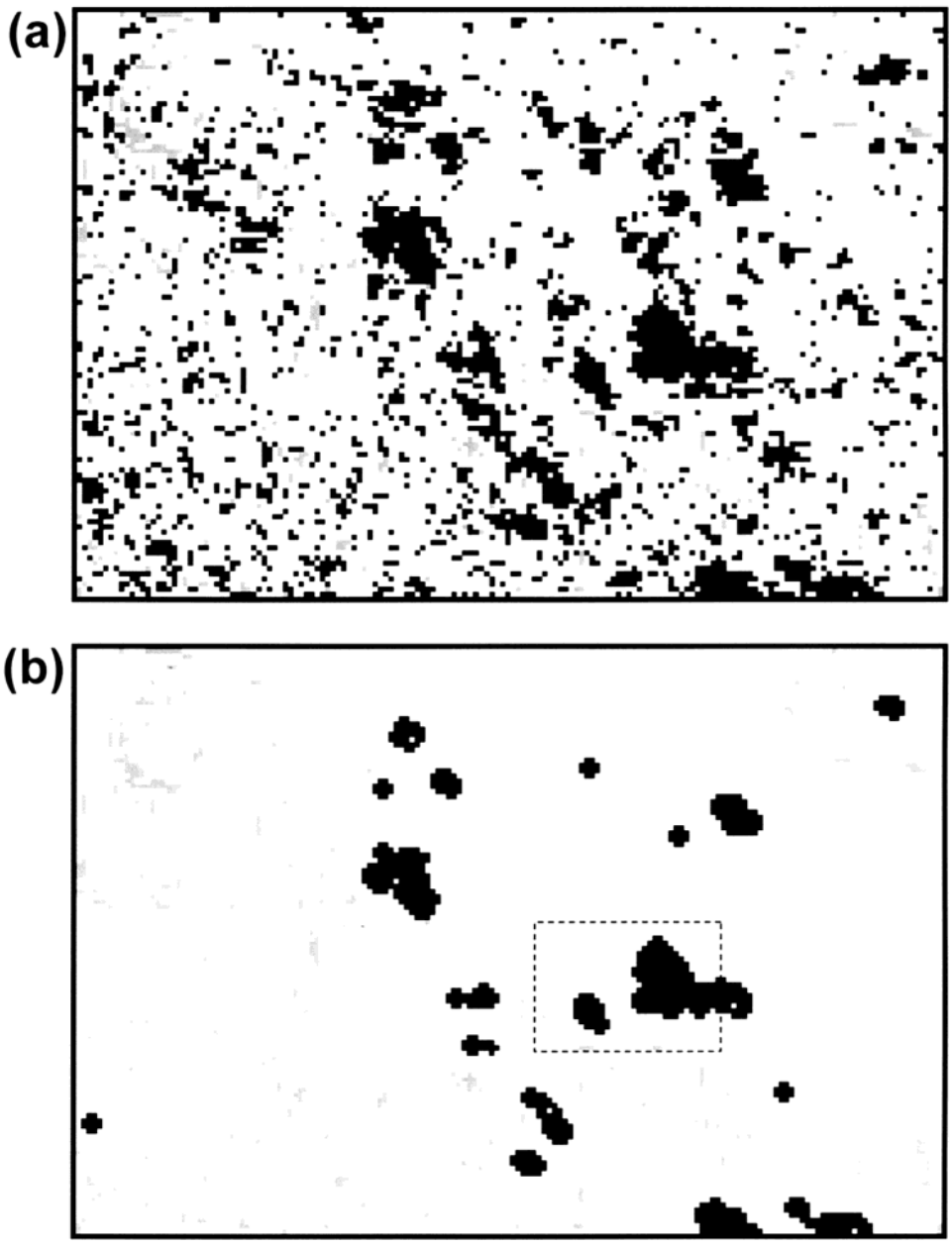

Figure 5. Assignment maps of a typical TEM micrograph before and after filtering. (a) Raw assignments of each of the 18 924 boxes comprising a micrograph: white, disorder; black, order; gray, unclear. (b) Same micrograph after applying the filtering procedure that reassigns isolated ordered boxes to disordered. The region depicted in Figure 4 is outlined by the dotted lines in part b.

N/R_{max} is 0.4, which is less than 2, so the algorithm assigns this region as ordered. For the LFT of box 2, $\log(A_{max}) = 12.7$, $R_{max} = 4.1$, and $N = 30$. The value of N/R_{max} is 7.3, which is greater than 2, so the algorithm assigns this region as disordered.

Applying the algorithm described above to each box in each micrograph yields assignment maps that distinguish between ordered, disordered, and unclear regions, such as the one shown in Figure 5a, which depicts the whole micrograph from which the fragment shown in Figure 4 was extracted. Each "pixel" on these maps represents the result from the analysis of one 32×32 pixel box in the original image. Examining such maps, one notices single isolated ordered pixels (or very small isolated groups of ordered pixels) obtained in the middle of disordered regions. Visual inspection of the corresponding regions on each micrograph suggested that they were in fact disordered. We attribute these pixels to noise, graininess, or poor focusing in the images and/or limitations of the algorithm used to process the images. The data in Figure 5a were thus subjected to a filtering process to reassign these isolated ordered pixels. A Fortran program was written to examine the neighborhood of each ordered box. If three or fewer of the eight boxes surrounding a given ordered box were ordered, then that box was reassigned as disordered. The filtration process was repeated seven times; additional filtering led to no further changes in box assignments. The results of this filtering process are shown in Figure 5b. A comparison of the raw image and filtered map indicates that the filtered analysis produces a conservative but faithful estimate of ordered regions in each micrograph. Note that the incorrect inclusion of a large number of isolated ordered pixels would lead to substantial errors in our estimate of the average grain size.

The volume fraction of ordered grains (ϕ) is simply the fraction of ordered boxes in the 53/56 micrographs [ϕ = no. of ordered boxes/(no. of ordered boxes + no. of disordered boxes); we ignore unclear boxes]. We obtained $\phi_{early} = 0.032$ and $\phi_{late} = 0.07$. These values are based on the examination of approximately 10^6 boxes for each sample; the difference between ϕ_{late} and ϕ_{early} is thus well outside statistical uncertainty. The ratio $\phi_{late}/\phi_{early} = 2.1$. The values of ϕ were affected by the value of the N/R_{max} cutoff. Values of the cutoff in the 2.5−3.0 range produced larger volume fractions of ordered regions, although the ratio ϕ_{late}/ϕ_{early} remained unchanged. The formula for calculating ϕ assumes a uniform structure throughout the area and thickness of a box. If portions of the microtomed slice are so thick as to encompass both ordered and disordered regions within one box, the assignment of that box would probably be assigned to the local structure (order or disorder) that occupies most of the thickness. This might give rise to occasional incorrect assignments, but on average, it would not produce a significant error in the determination of ϕ.

We define d_{app} to be the measured (or apparent) periodic length scale in each of the ordered and disordered boxes. The value of d_{app} is $32/R_{max}$ in units of pixels or $1.75 \times 32/R_{max}$ in units of nanometers. Because of the digital nature of the LFTs, only certain discrete, unequally spaced values of the period d_{app} can be obtained by this procedure. It was therefore necessary to employ bins corresponding to period ranges of unequal length, to ensure that all bins included at least one obtainable period value. Parts a and b of Figure 6 show the distribution (probability density) of d_{app} in ordered and disordered regions of the S_{early} sample, respectively. This quantity is the fraction of boxes whose period falls within a given period range divided by the length of that range. Parts a and b of Figure 7 show the distribution of d_{app} in ordered and disordered regions of the S_{late} sample, respectively. In both S_{early} and S_{late}, the distribution of d_{app} values is sharply peaked at 13 ± 1 nm, irrespective of whether we examine ordered regions (Figures 6a and 7a) or disordered regions (Figures 6b and 7b). SAXS and SANS studies of lamellar samples near the order−disorder transition have indicated that the d spacing of weakly ordered lamellae and the length scale of the periodic concentration fluctuations in the disordered state close to the order−disorder transition are not very different.[1−5] The data in Figures 6 and 7 are consistent with this observation. In Figure 8 we show small-angle X-ray scattering data from S_{late}.[29] We see a sharp scattering peak at $q = 0.45$ nm^{-1}, indicating a spatial period $d = 14$ nm ($d = 2\pi/0.45$). The agreement between TEM and SAXS seen in Figures 7 and 8 is reassuring. It also rules out the possibility of large-scale distortions of the sample during microtoming and staining.

For ordered regions of a sample, the local lamellar normal has polar and azimuthal angles, $\theta(\mathbf{r})$ and $\varphi(\mathbf{r})$, measured relative to a z-axis defined by the direction normal to the microtoming plane and an arbitrary x-axis in the microtoming plane. For grains with polar angle θ significantly different from 90°, d_{app} will be larger than the actual spacing. For a collection of randomly oriented grains, most grains will be sliced so that the lamellar planes are approximately perpendicular to the slice plane, because a much larger volume of solid angle is covered as a narrow cone with axis near $\theta = 90°$ sweeps

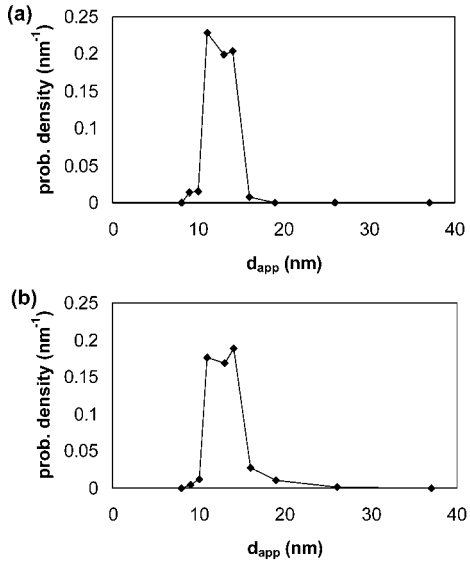

Figure 6. Probability density of apparent periodicity d_{app} of electron micrographs in sample S_{early}: (a) ordered regions; (b) disordered regions. The periodicity is peaked at 13 ± 1 nm in both regions.

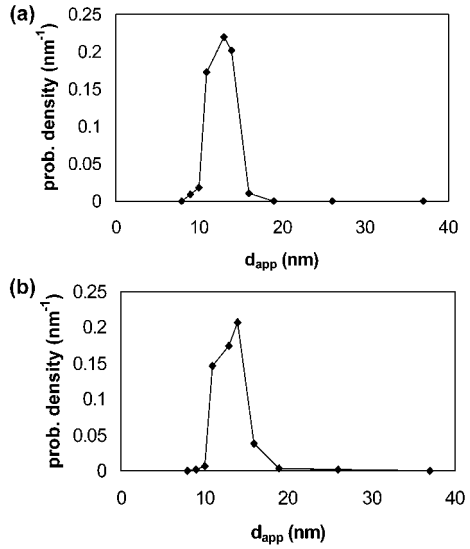

Figure 7. Probability density of apparent periodicity d_{app} of electron micrographs in sample S_{late}: (a) ordered regions; (b) disordered regions. The periodicity is peaked at 13 ± 1 nm in both regions.

from $\varphi = 0°$ to 360° than for a cone with axis near $\theta = 0°$. The probability of finding lamellar grains with polar angle θ is thus proportional to sin θ. Thus, the TEM images are dominated by lamellae with $\theta = 90°$, and the dominant d_{app} is coincident the true d spacing of the lamellae.

We now compute the correlation function from the TEM images. Recall that the DPLS data indicated the presence of two correlation lengths: $\omega_{||}$ in the direction of the optic axis and $\omega_{\perp}$ perpendicular to it. A micrograph represents a two-dimensional slice of the grain structure of a sample. Generally speaking, the local optic axis direction will not lie in the micrograph plane. However, the projection of the optic axis of a grain onto the plane of the micrograph is perpendicular to the striped pattern and is thus easily determined. We obtain the correlation function of the grain structure in two steps. We first compute the 2-dimensional correlation lengths along and perpendicular to the optic axis

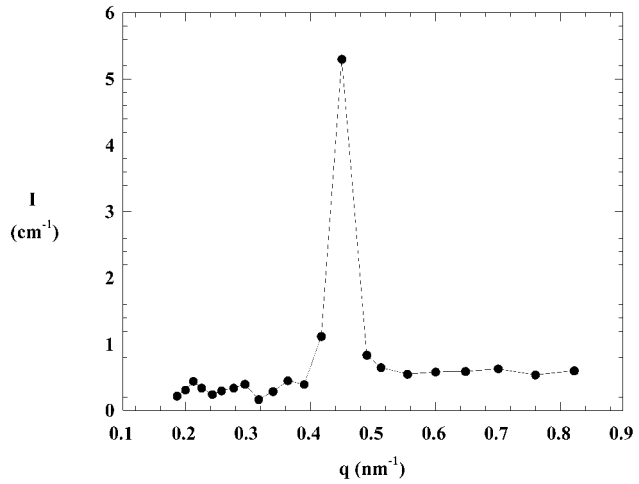

Figure 8. Small-angle X-ray scattering data from a duplicate of sample S_{late} at room temperature, indicating an average *d* spacing of 14 nm.

projection. We then correct for the 3-dimensional nature of the grains.

Our LFT procedure produces a matrix of local azimuthal angles, $\varphi(\mathbf{r})$, that describes the orientation of the projection of the optic axis in the micrograph plane. An example of such a matrix is shown in Figure 9, which corresponds to the micrograph in Figure 4a. As shown in ref 10, this matrix can be used to calculate the lamellar orientation correlation function, $C(\mathbf{r})$:

$$C(|\mathbf{r}' - \mathbf{r}''|) = (15/8)\langle \sin^2\theta(\mathbf{r}')\sin^2\theta(\mathbf{r}'')\rangle\langle\cos\{2[\varphi(\mathbf{r}') - \varphi(\mathbf{r}'')]\}\rangle \approx \langle\cos\{2[\varphi(\mathbf{r}') - \varphi(\mathbf{r}'')]\}\rangle \quad (5)$$

where the brackets $\langle ... \rangle$ indicate an average over all pairs of points $\mathbf{r}'$ and $\mathbf{r}''$ in ordered regions of the micrograph. Recall that boxes that fall within ordered regions were identified using the algorithm described previously. To examine the possibility of grain anisotropy, we evaluate two different correlation functions, $C_{\parallel}$ and $C_{\perp}$, corresponding to correlations in the direction of the optic axis projection and perpendicular to the optic axis projection, respectively. The former is calculated by averaging only over pairs of points $\mathbf{r}'$ and $\mathbf{r}''$ that satisfy the condition that the vector $\mathbf{r}' - \mathbf{r}''$ is parallel to the optic axis projection at point $\mathbf{r}'$ or point $\mathbf{r}''$, within a certain tolerance, chosen here to be 5°. (The resulting correlation function is insensitive to the particular value of the tolerance chosen.) The latter is calculated by averaging only over pairs of points $\mathbf{r}'$ and $\mathbf{r}''$ that satisfy the condition that the vector $\mathbf{r}' - \mathbf{r}''$ is perpendicular to the optic axis projection at point $\mathbf{r}'$ or point $\mathbf{r}''$, within a certain tolerance (also chosen to be 5°). This procedure was carried out for every pair of points in ordered regions of the 53/56 independent micrographs of each sample, and we thus obtained $C_{\parallel}(r)$ and $C_{\perp}(r)$.

Both correlation functions were found to be approximately exponentially decaying. The functions tend to level off to constant values at distances greater than about 0.5 μm (see inset in Figure 10b). Each curve was fit to an exponential function of the form $\exp(-r/\kappa)$ for $r < 0.35$ μm, where κ is an exponential correlation length parameter. The average baselines for $r > 0.5$ μm were approximately 0.2 and 0.3 for S_{early} and S_{late}, respectively. The baselines are probably due to the limited sample size covered by the 53/56 micrographs giving rise to incomplete statistical averaging at each *r*, and we attach no significance to their magnitudes. The exponential correlation functions of S_{early} and S_{late} are shown in parts a and b of Figure 10, respectively. In both samples, the correlation length in the direction of the optic axis, $\kappa_{\parallel}^{2D}$, is larger than the correlation length in direction perpendicular to the optic axis, $\kappa_{\perp}$. The resulting correlation lengths parallel and perpendicular to the optic axis projection, $\kappa_{\parallel}^{2D}$ and $\kappa_{\perp}$, respectively, are listed in Table 1. The values of $\kappa_{\parallel}^{2D}$ and $\kappa_{\perp}$ are based on 10^8 pairs of boxes. Thus, the differences between the grain size parameters of S_{early} and S_{late}, given in Table 1, are well outside statistical uncertainty.

We now address the issue of estimating 3D correlation functions from 2D data. As discussed above, the apparent optic axis direction associated with a region of a TEM micrograph is actually the projection of the optic axis on the slice plane. On the other hand, the direction that appears to be perpendicular to the optic axis on a TEM micrograph is also perpendicular to the optic axis in the 3D sample from which the microtomed section

*	*	*	*	*	*	*	*	*	*	*	*	*	*	*	*	*	*	*	*
*	*	*	*	*	*	*	*	*	*	*	*	76	76	*	*	*	*	*	*
*	*	*	*	*	*	*	*	*	*	*	76	76	76	76	*	*	*	*	*
*	*	*	*	*	*	*	*	*	*	*	90	90	90	90	90	*	*	*	*
*	*	*	*	*	*	*	*	*	*	*	104	104	104	104	104	104	*	*	*
*	*	*	*	*	*	*	*	*	*	*	*	117	117	117	117	127	127	117	117
*	*	*	*	*	*	63	*	*	*	*	117	117	117	117	117	117	117	117	117
*	*	*	*	*	76	76	76	*	*	*	117	117	117	117	117	117	117	104	104
*	*	*	*	*	76	76	76	*	*	*	*	*	*	104	*	*	90	*	*
*	*	*	*	*	*	76	76	76	*	*	*	*	*	*	*	*	*	*	*
*	*	*	*	*	*	*	*	*	*	*	*	*	*	*	*	*	*	*	*
*	*	*	*	*	*	*	*	*	*	*	*	*	*	*	*	*	*	*	*
*	*	*	*	*	*	*	*	*	*	*	*	*	*	*	*	*	*	*	*

Figure 9. Typical matrix of local azimuthal angles, $\varphi(\mathbf{r})$, that describes the orientation of the projection of the optic axis in the ordered regions in the micrograph (*xy*) plane. The corresponding micrograph is shown in Figure 4. The asterisks denote disordered or unclear regions. For the sake of clarity, every other calculated angle is shown.

Table 1. Correlation Lengths and Volume Fractions of Ordered Grains from Depolarized Light Scattering and Electron Microscopy[a]

	depolarized light scattering				transmission electron microscopy					
sample	$\omega_{\|}$ (μm)	$\omega_{\perp}$ (μm)	$\omega_{\|}/\omega_{\perp}$	ϕ_{late}/ϕ_{early}	$\kappa_{\|}^{2D}$ (μm)	$\kappa_{\|}$ (μm)	$\kappa_{\perp}$ (μm)	$\kappa_{\|}/\kappa_{\perp}$	ϕ	ϕ_{late}/ϕ_{early}
S_{early}	1.8	0.9	2.0		0.47	0.61	0.32	1.9	0.032	
S_{late}	2.4	1.6	1.5	1.9	0.69	0.81	0.51	1.6	0.07	2.1

[a] ω and κ are Gaussian and exponential correlation lengths, respectively, and ϕ is the volume fraction of ordered grains. Uncertainties in the fitted κ values are ± 0.01.

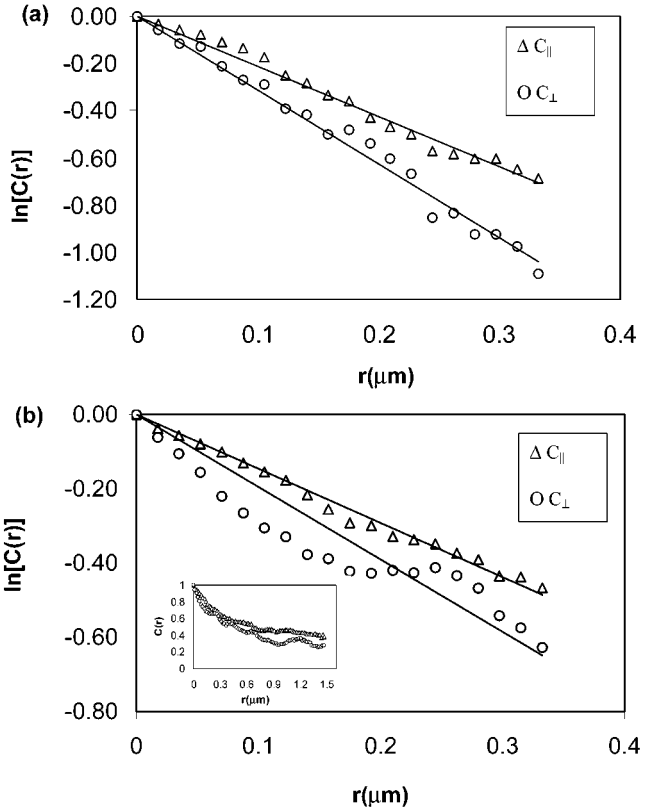

Figure 10. Correlation function of samples (a) S_{early} and (b) S_{late} in directions parallel (triangles) and perpendicular (circles) to the local optic axis. $C(r)$ is defined by the average of eq 5 over 53/56 micrographs for each of the samples. [The complete curves of $C(r)$ vs r for S_{late} are shown in the inset in part b.] Exponential fits of the first 20 points of each $C(r)$ give the correlation lengths $\kappa_{\|}^{2D}$ and $\kappa_{\perp}$.

was obtained. Thus, the $\kappa_{\perp}$ values calculated from 2D projections are identical to the corresponding 3D correlation lengths, but the calculated $\kappa_{\|}^{2D}$ values are smaller than the corresponding 3D lengths (assuming $\kappa_{\|} > \kappa_{\perp}$) because they include directions that are somewhere between parallel and perpendicular to the optic axis. Some analysis is required to relate $\kappa_{\|}^{2D}$ to its 3D counterpart, $\kappa_{\|}$.

The micrographs are taken to lie in the $x-y$ plane of a laboratory reference frame. We assume that $\{\xi, \eta, \zeta\}$ represents the coordinates of a grain reference frame where the optic axis is along ζ. In this frame, we assume the full 3D correlation function has the exponential form

$$C(\xi,\eta,\zeta) = \exp[-\{(\xi^2 + \eta^2)/\kappa_{\perp}^2 + \zeta^2/\kappa_{\|}^2\}^{1/2}] \quad (6)$$

Note that eq 6 reduces to simple exponentials along the directions $\|$ and $\perp$ to the optic axis and are thus consistent with the experimental data in Figure 10. We also define the laboratory x-axis to coincide with the projection of the grain optic axis onto the $x-y$ plane. In that case, the y-axis is perpendicular to the grain optic

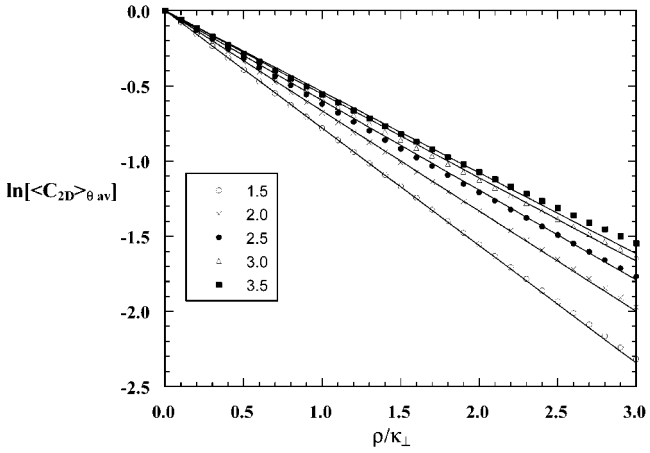

Figure 11. θ-averaged 2-dimensional correlation function $\langle C_{2D}\rangle_{\theta average}$ vs normalized distance $\rho/\kappa_{\perp}$ in the micrograph plane for different values of $\kappa_{\|}/\kappa_{\perp}$ indicated in the legend. Symbols represent full calculations using eq 11. Dashed lines are least-squares exponential fits to the full calculations that give $\kappa_{\|}^{2D}$.

axis, and without any loss of generality, we can define the grain's η-axis to coincide with the y-axis. Assuming the optic axis makes an angle θ with the z-axis, the correlation function can be represented as

$$C(x,y,z) = \exp[-\{(x\cos\theta - z\sin\theta)^2 + y^2)/\kappa_{\perp}^2 + (z\cos\theta + x\sin\theta)^2/\kappa_{\|}^2\}^{1/2}] \quad (7)$$

The projection of this correlation function onto the $x-y$ plane, C_{2D}, is, in polar coordinates, given by

$$C_{2D}(\rho,\phi,\theta) = \exp[-\rho\{\sin^2\phi/\kappa_{\perp}^2 + \cos^2\phi(\sin^2\theta/\kappa_{\|}^2 + \cos^2\theta/\kappa_{\perp}^2)\}^{1/2}] \quad (8)$$

where $x = \rho\cos\phi$ and $y = \rho\sin\phi$. Along the y-axis ($\phi = \pi/2$), the 2D correlation function is a simple exponential with correlation length $\kappa_{\perp}$ and is independent of the angle θ that the optic axis makes with the z-axis:

$$C_{2D}(\rho,\pi/2,\theta) = \exp[-\rho/\kappa_{\perp}] \quad (9)$$

Along the x-axis we have

$$C_{2D}(\rho,0,\theta) = \exp[-\rho(\sin^2\theta/\kappa_{\|}^2 + \cos^2\theta/\kappa_{\perp}^2)^{1/2}] = \exp[-(\rho/\kappa_{\perp})\{(\sin^2\theta/(\kappa_{\|}/\kappa_{\perp})^2 + \cos^2\theta)\}^{1/2}] \quad (10)$$

The average of this function over θ cannot be represented by a simple analytic function, but the integration can be performed numerically. However, as we shall see below, the results match well to a simple exponential:

$$\langle C_{2D}\rangle_{\theta average} = \int C_{2D}(\rho,0,\theta)\sin\theta\,d\theta/\int\sin\theta\,d\theta \approx \exp[-(\rho/\kappa_{\perp})/(\kappa_{\|}^{2D}/\kappa_{\perp})] = \exp(-\rho/\kappa_{\|}^{2D}) \quad (11)$$

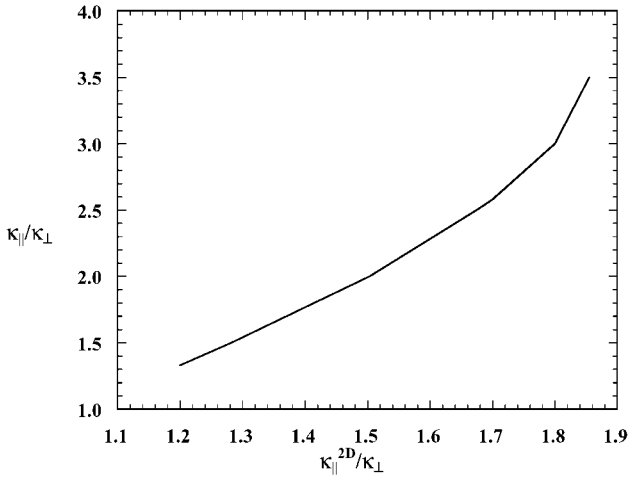

Figure 12. Dependence of $\kappa_{||}/\kappa_{\perp}$, the average anisotropy of the 3-dimensional grain, vs $\kappa_{||}^{2D}/\kappa_{\perp}$, the average anisotropy measured in a 2-dimensional slice of the same sample.

In the semilog plot in Figure 11, the symbols represent calculations of $\langle C_{2D}\rangle_{\theta average}$ vs $\rho/\kappa_{\perp}$ for selected values of $\kappa_{||}/\kappa_{\perp}$. The approximate linearity of each data set indicates that $\langle C_{2D}\rangle_{\theta average}$ can be approximated by a simple exponential.

For each data set in Figure 11, we also give a straight line that represents the least-squares exponential approximation for $\langle C_{2D}\rangle_{\theta average}$. It is thus clear that $\kappa_{||}^{2D}/\kappa_{\perp}$ is the measured average grain anisotropy measured in two-dimensional projections of a three-dimensional sample with true average anisotropy of $\kappa_{||}/\kappa_{\perp}$. Figure 12 shows the dependence of $\kappa_{||}/\kappa_{\perp}$ on $\kappa_{||}^{2D}/\kappa_{\perp}$. It is evident from Figure 12 that the average anisotropy seen in the projected plane is significantly lower than that present in the 3-dimensional structure. The difference between $\kappa_{||}/\kappa_{\perp}$ and $\kappa_{||}^{2D}/\kappa_{\perp}$ increases rapidly as the grains become more anisotropic. For S_{early}, $\kappa_{||}^{2D}/\kappa_{\perp} = 1.47$ while for S_{late}, $\kappa_{||}^{2D}/\kappa_{\perp} = 1.35$. From Figure 12 we estimate that $\kappa_{||}/\kappa_{\perp} = 1.9$ for S_{early} and $\kappa_{||}/\kappa_{\perp} = 1.6$ for S_{late}. The correlation lengths, $\kappa_{||}^{2D}$, $\kappa_{||}$, and $\kappa_{\perp}$, based on TEM data, are given in Table 1.

6. Gaussian and Exponential Correlation Functions

In a previous paper,[15] where DPLS and TEM data from samples filled with ideal grains were studied, two functional forms were used to describe the correlations within each grain: exponential [$C(r) = \exp(-r/\kappa)$] and Gaussian [$C(r) = \exp(-r^2/2\omega^2)$]. It was found that the DPLS data were consistent with both exponential and Gaussian correlation functions provided κ and ω were treated as adjustable parameters. In the samples studied in ref 15, $\omega/\kappa = 1.8 \pm 0.1$. That ω and κ are unequal is not surprising; if we equate the first moments $\langle r\rangle$ of these two distributions, we get the relation $\omega/\kappa = (3/2)\sqrt{\pi/2} = 1.9$, suggesting that the form of the scattering pattern in the DPLS experiment is sensitive mainly to the first moment (i.e., the average grain size), rather than the detailed functional form, of $C(r)$. The TEM data, however, were only consistent with an exponential correlation function. The κ values obtained from TEM were a factor of 2 smaller than the κ values obtained from DPLS.

For the case of nonideal, ellipsoidal grains, we were only able to evaluate the integrals needed for computing $I(q,\mu)$ for the case of Gaussian correlation or shape functions. We are thus forced to use Gaussian functions to analyze the DPLS data from anisotropic grains even though we expect exponential functions to be more appropriate.[30]

7. Comparing DPLS and TEM Results

A comparison of the analyses of grain structure using DPLS and TEM data is shown in Table 1. Qualitatively, the two techniques are in remarkable agreement, especially when one considers the differences between the two techniques. The ratio ϕ_{late}/ϕ_{early} is 1.9 based on DPLS and 2.1 based on TEM. Both experimental techniques indicate that grains are, on average, longer in the direction of the optic axis. We define the grain anisotropy ratio α to be the ratio of the grain size parallel to the optic axis to that perpendicular to the optic axis. For S_{early}, α based on DPLS is 2.0 while that based on TEM is 1.9. For S_{late}, α based on DPLS is 1.5 while that based on TEM is 1.6. *The measured value of the anisotropy factor of weakly ordered lamellar grains grown in the vicinity of the order−disorder transition is thus about 2.*

The anisotropy factor that we find appears to be significantly lower than that suggested in ref 5 for lamellar grains. The representative isolated grain reported in Figure 5 of ref 5 exhibits an anisotropy ratio $\alpha = 4$. The micrographs shown in Figure 7 of ref 5 show grains with even larger anisotropies. However, it is difficult to make any quantitative statistical generalizations from such a small sample of micrographs, especially when those micrographs were probably selected specifically to demonstrate the presence of highly anisotropic grains. From our own TEM data, visual inspection of Figure 3a reveals a grain with an anisotropy greater than 4. However, the statistical analysis of 53 early micrographs yields a considerably lower anisotropy of about 2.

From Table 1 it is clear that the main discrepancy between TEM and DPLS results is in the absolute magnitude of the correlation lengths. The Gaussian light scattering lengths, ω, are consistently about 3 times larger than the corresponding exponential microscopy lengths, κ. After correcting for the use of Gaussian correlation or shape functions in the analysis of the DPLS data using the approximate relation $\kappa \approx \omega/2$, the light scattering lengths are consistently 50% larger than the corresponding microscopy lengths. A similar underestimate of correlation lengths by microscopy was seen in earlier work on ideal grains.[15] The discrepancy is not surprising when one considers the complexity of grain structure in partially ordered block copolymer samples and the fact that distinguishing between order and disorder is nontrivial given the imperfections of TEM micrographs.

8. Concluding Remarks

The structure of partially ordered, lamellar block copolymer samples was studied by a combination of depolarized light scattering and transmission electron microscopy. An algorithm for analyzing the TEM micrographs partially filled with anisotropic grains was developed on the basis of a local Fourier transform analysis. This analysis led to the establishment of quantitative criteria for distinguishing between ordered and disordered regions. In addition, correlation functions that describe the orientation of the lamellae along the optic axis and perpendicular to it were computed.

Both light scattering and electron microscopy indicate that, on average, the grains are longer in the direction of the optic axis by a factor of about 2. The ratio of grain volume fraction ϕ_{late}/ϕ_{early} determined from light scattering and electron microscopy are in reasonable agreement. The absolute magnitudes of grain sizes determined by light scattering are approximately 50% larger than those determined by microscopy. This discrepancy indicates the need for better analysis of both DPLS and TEM data.

The TEM analysis could be improved by imaging larger contiguous areas so that each data set contains a larger number of randomly oriented grains. This would enable a study of intergrain correlations that are inferred from light scattering studies and may also reduce the baseline in the measured correlation functions. Automating the data acquisition and analysis scheme that we have developed will lead to larger samples and more accurate ensemble averages. The TEM results clearly show the limitations of using Gaussian correlation functions for describing the grain structure within ordered block copolymers. Exponential correlation functions appear to be more realistic; we have not been able to obtain usable expressions for the DPLS profiles from anisotropic grain clusters. We will address some of these limitations in future work. We feel, however, that the electron microscopy data presented here provide substantial confirmation of previously developed models for the analysis of depolarized light scattering data from ordered block copolymers.

Acknowledgment. Financial support provided by the National Science Foundation (DMR-9901951), and the Dreyfus Foundation, is gratefully acknowledged. The UNICAT facility at the Advanced Photon Source (APS) is supported by the University of Illinois at Urbana−Champaign, Materials Research Laboratory, U.S. Department of Energy (DOE), The State of Illinois-IBHE-HECA, the National Science Foundation, the Oak Ridge National Laboratory (DOE), the National Institute of Standards and Technology (U.S. Department of Commerce), and UOP LLC. The APS is supported by the U.S. DOE, BES, Office of Energy Research, under Contract W-31-109-ENG-38. The assistance of Dr. Gabrielle Long is gratefully acknowledged.

References and Notes

(1) Leibler, L. *Macromolecules* **1980**, *13*, 1602.
(2) Fredrickson, G. H.; Helfand, E. *J. Chem. Phys.* **1987**, *87*, 697.
(3) Bates, F. S.; Rosedale, J. H.; Fredrickson, G. H. *J. Chem. Phys.* **1990**, *92*, 6255.
(4) Mori, K.; Okawara, A.; Hashimoto, T. *J. Chem. Phys.* **1996**, *104*, 7765.
(5) Sakamoto, N.; Hashimoto, T. *Macromolecules* **1998**, *31*, 3815.
(6) Gido, S. P.; Thomas, E. L. *Macromolecules* **1994**, *27*, 6137.
(7) Kawasaki, K.; Onuki, A. *Phys. Rev. A* **1990**, *42*, 3664.
(8) Csernica, J.; Baddour, R. F.; Cohen, R. E. *Macromolecules* **1989**, *22*, 1493.
(9) Polis, D. L.; Winey, K. I. *Macromolecules* **1998**, *31*, 3617.
(10) Park, M.; Harrison, C.; Chaikin, P. M.; Register, R. A.; Adamson, D. *Science* **1997**, *276* 1401.
(11) Fink, Y.; Urbas, A. M.; Bawendi, M. G.; Joannopoulos, J. D.; Thomas, E. L. *IEEE J. Lightwave Technol.* **1999**, *17*, 1963.
(12) Myers, R. T.; Cohen, R. E.; Bellare, A. *Macromolecules* **1999**, *32*, 2706.
(13) Balsara, N. P.; Garetz, B. A.; Dai, H. J. *Macromolecules* **1992**, *25*, 6072.
(14) Garetz, B. A.; Newstein, M. C.; Dai, H. J.; Jonnalagadda, S. V.; Balsara, N. P. *Macromolecules* **1993**, *26*, 3151.
(15) Garetz, B. A.; Balsara, N. P.; Dai, H. J.; Wang, Z.; Newstein, M. C.; Majumdar, B. *Macromolecules* **1996**, *29*, 4675.
(16) Dai, H. J.; Balsara, N. P.; Garetz, B. A.; Newstein, M. C. *Phys. Rev. Lett.* **1996**, *77*, 3677.
(17) Balsara, N. P.; Garetz, B. A.; Chang, M. Y.; Dai, H. J.; Newstein, M. C.; Goveas, J. L.; Krishnamoorti, R.; Rai, S. *Macromolecules* **1998**, *31*, 5309.
(18) Balsara, N. P.; Garetz, B. A.; Newstein, M. C.; Bauer, B. J.; Prosa, T. J. *Macromolecules* **1998**, *31*, 7668.
(19) Newstein, M. C.; Garetz, B. A.; Balsara, N. P.; Chang, M. Y.; Dai, H. J. *Macromolecules* **1998**, *31*, 64.
(20) Wang, H.; Newstein, M. C.; Chang, M. Y.; Balsara, N. P.; Garetz, B. A. *Macromolecules* **2000**, *33*, 3719.
(21) Beyer, F. L.; Bueschl, C.; Gido, S. P.; Iatrou, H.; Uhrig, D.; Mays, J. W.; Chang, M. Y.; Garetz, B. A.; Balsara N. P.; Tan, N. B. *Macromolecules* **2000**, *33*, 2039.
(22) Harrison, C.; et al. *Macromolecules* **2000**, *33*, 857.
(23) Harrison, C.; Adamson, D. H.; Cheng, Z.; Sebastian, J. M.; Sethuraman, S.; Huse, D. A.; Register, R. A.; Chaikin, P. M. *Science* **2000**, *290*, 1558.
(24) Hahm, J.; Lopes, W. A.; Jaeger, H. M.; Sibener, S. J. *J. Chem. Phys.* **1998**, *109*, 10111.
(25) Lin, C. C.; Jonnalagadda, S. V.; Kesani, P. K.; Dai, H. J.; Balsara, N. P. *Macromolecules* **1994**, *27*, 7769.
(26) Long, G. G.; Allen, A. J.; Ilavsky, J.; Jemian, P. R.; Zschak, P. In *Proceedings: Synchrotron Radiation Instrumentation: Eleventh US National Conference*; Pianetta, P., Ed.; 2000; American Institute of Physics: Melville, NY, pp 183−187.
(27) Lake, J. A. *Acta Crystallogr.* **1967**, *23*, 91.25.
(28) Stein, R. S. In *Electromagnetic Scattering*; Kerker, M., Ed.; Pergamon Press: Oxford, U.K., 1963; p 439.
(29) The samples studied in this paper did not exhibit the USAXS signatures reported in ref 12. We thus focus on the scattering profile in the vicinity of the Bragg peaks corresponding to the lamellar spacing. This may be due to the fact that the present samples were partially ordered, while those studied in ref 12 were fully ordered.
(30) We have recently succeeded in evaluating the integrals needed to compute $I(q,\mu)$ for the case of uncorrelated, ellipsoidal grains using exponential correlation functions. Over a wide range of grain anisotropy ratios, the relationship $\omega/\kappa \approx 2$ continues to hold, and we expect that this relationship holds for ellipsoidal grain clusters as well.

MA0201025